Steady-State Confinement of Electron Plasmas Using Trivelpiece-Gould Modes Excited by a "Rotating Wall"

F. Anderegg, E.M. Hollmann, and C.F. Driscoll

Department of Physics
and
Institute for Pure and Applied Physical Sciences
University of California at San Diego, la Jolla, CA 92093-0319 USA

Abstract.

A "rotating wall" electric field can give steady-state confinement of more than 10^9 charges in a Penning-Malmberg trap at 4 Tesla. For both pure ion plasmas and pure electron plasmas, the torque exerted on the plasma by the rotating wall exhibits peaks at the frequencies of $k_z \neq 0$ Trivelpiece-Gould modes. As expected, modes with $\omega > \omega_R$ (i.e. propagating faster than the plasma rotation) give positive torque and cause plasma compression; and modes with $\omega < \omega_R$ give adverse torque and cause plasma expansion. By increasing the frequency of the rotating wall, we observed a plasma central density compression of about a factor of 20. These techniques may be useful for a variety of trapping experiments.

Nonneutral electron or ion plasmas confined in Penning-Malmberg traps have inherent confinement times which are long, but finite. In practice, background neutral gas and small confinement field asymmetries exert a drag on the rotating plasma, causing slow radial expansion and eventual particle loss. Previous work [1] on small ion plasmas has demonstrated radial compression and steady-state confinement using laser techniques to apply a torque which counteracts the drag on the plasma. However, there is considerable interest in containment of elementary particles, including antimatter [2], where laser techniques are not applicable.

Previously, modest density and angular momentum changes of electron plasmas were reported [3,4] when applied dipolar electric fields excited a plasma mode, but strong heating and background gas ionization made the technique impractical at low magnetic fields ($B \leq 400$G). In other experiments, this background gas ionization is used to maintain a steady state electron target for high energy beams [5]. Recently, these "rotating wall" electric fields applied to the end of a column of 10^9 Mg^+ ions have been shown to give steady-state confinement and compression up to 20% of the Brillouin density limit [6].

In this paper, we describe electron plasmas confined by rotating dipole ($m_\theta = 1$) and quadrupole ($m_\theta = 2$) electric fields applied at one end of the plasma column. We show that the rotating wall fields apply a torque which can be used to compress or expand the plasma, and the torque is shown to arise from Trivelpiece-Gould plasma modes. The rotating wall fields also cause plasma heating: for electron plasmas the cyclotron radiation cooling at $B = 4$T keeps the plasma temperature low; for ion plasmas, collisions with neutral gas or laser cooling keeps the ion temperature low. The IV apparatus [7] used here normally contains Mg^+ ions which are continuously diagnosed by laser-induced fluorescence. When containing electrons, the apparatus operates in a standard inject/hold-and-manipulate/dump-and-measure cycle [8].

Figure 1 shows the Penning-Malmberg trap consisting of cylindrical electrodes of radius $R_w = 2.86$ cm in

CP457, *Trapped Charged Particles and Fundamental Physics*
edited by Daniel H. E. Dubin and Dieter Schneider

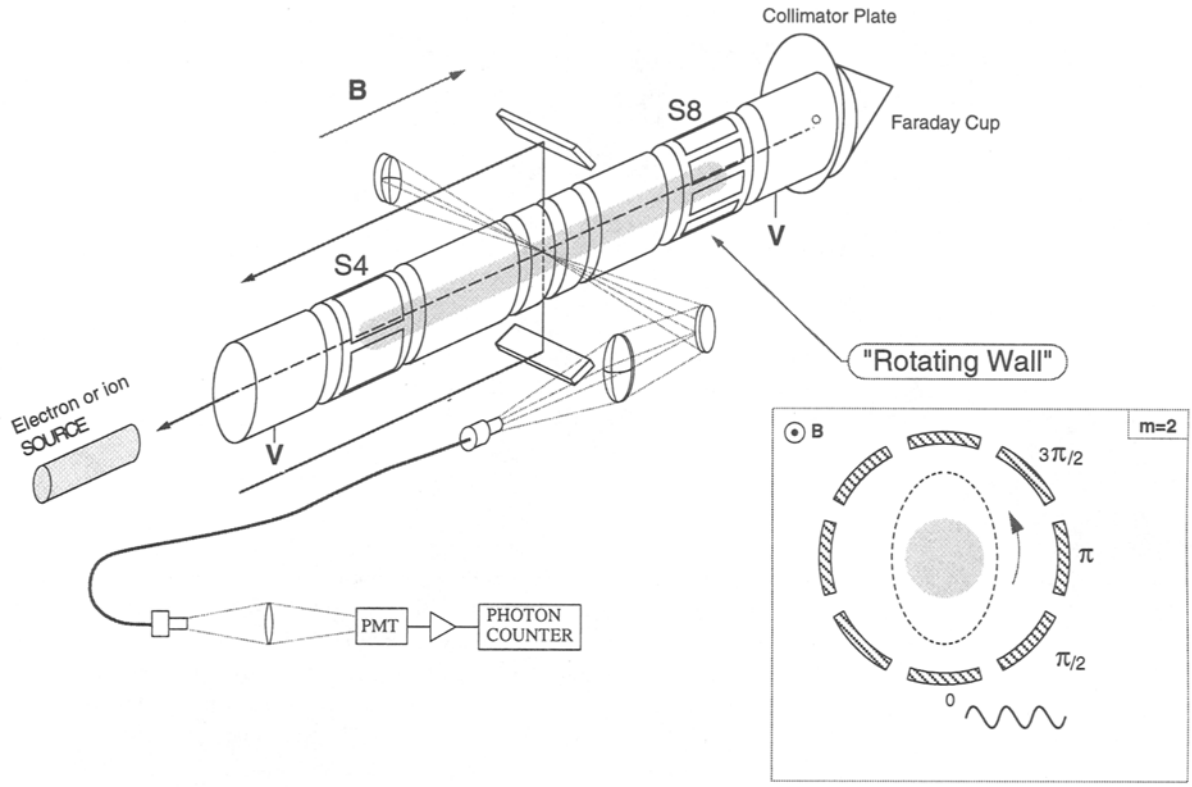

Fig. 1. Schematic diagram of the cylindrical trap, with inset representing the rotating wall drive on sectored cylinder S8.

ultra-high vacuum ($P \approx 3 \times 10^{-9}$ Torr, 97% H_2), in a uniform axial magnetic field ($B = 4\mathrm{T}\hat{z}$). Electron injection from a thoriated tungsten filament gives $N_{\mathrm{tot}} \approx 3 \times 10^9$ electrons in a column of length $L_p \approx 35$ cm and radius $R_p \approx 0.27$ cm, with central density $n_0 \approx 4 \times 10^8$ cm^{-3}.

The electron plasma density profile $n(r)$ and an estimate of the thermal energy T are obtained by dumping the plasma axially and measuring the charge passing through a hole in a (rotatable) collimator plate [9]. Both measurements require shot-to-shot reproducibility of the injected plasma, and we typically obtain variability $\delta n/n \lesssim 1\%$.

The radial expansion or compression of the plasma is determined by changes in the total angular momentum $P_\theta \equiv \sum_j [m v_{\theta_j} r_j - eBr_j^2/2c] \approx -(eB/2c)\sum_j r_j^2$, with the sum over the N_{tot} particles. At low temperature and low density, the angular momentum in the electromagnetic field dominates, so conservation of angular momentum implies conservation of the mean-square radius $\sum_j r_j^2$ of the plasma.

In practice, inherent "background" asymmetries in the magnetic or electric confinement fields [10] exert a weak drag on the rotating plasma, causing a decrease in P_θ and a bulk expansion of the plasma. Measurements show that this "mobility" expansion rate scales roughly as $\tau_m^{-1} \equiv -(\dot{n}_0/n_0)_{\mathrm{bkg}} \approx (6 \times 10^{-4}\ \mathrm{sec}^{-1})(n_0/10^8\ \mathrm{cm}^{-3})^2$ for the electron columns described here ($L_R = 35$ cm, $B = 4$T). To maintain or compress the plasma, the rotating wall drive must supply a positive torque as large or larger than this drag; alternately, a reverse-rotating drive can substantially increase the background expansion rate.

The rotating wall drive consists of sinusoidal voltages $\Phi_{wj} = A_w \cos(m_\theta \theta_j - 2\pi f_s t)$ applied to the eight sectors at $\theta_j = 2\pi j/8$. Here, f_s is the signal generator frequency, and the wall perturbation effectively rotates at $f_w = f_s/m_\theta$.

We find that the applied drive couples to the plasma through discrete $k_z \neq 0$ Trivelpiece-Gould (T-G) plasma mode resonances [11]. Figure 2 shows the measured peaks in the compression rate versus drive frequency when

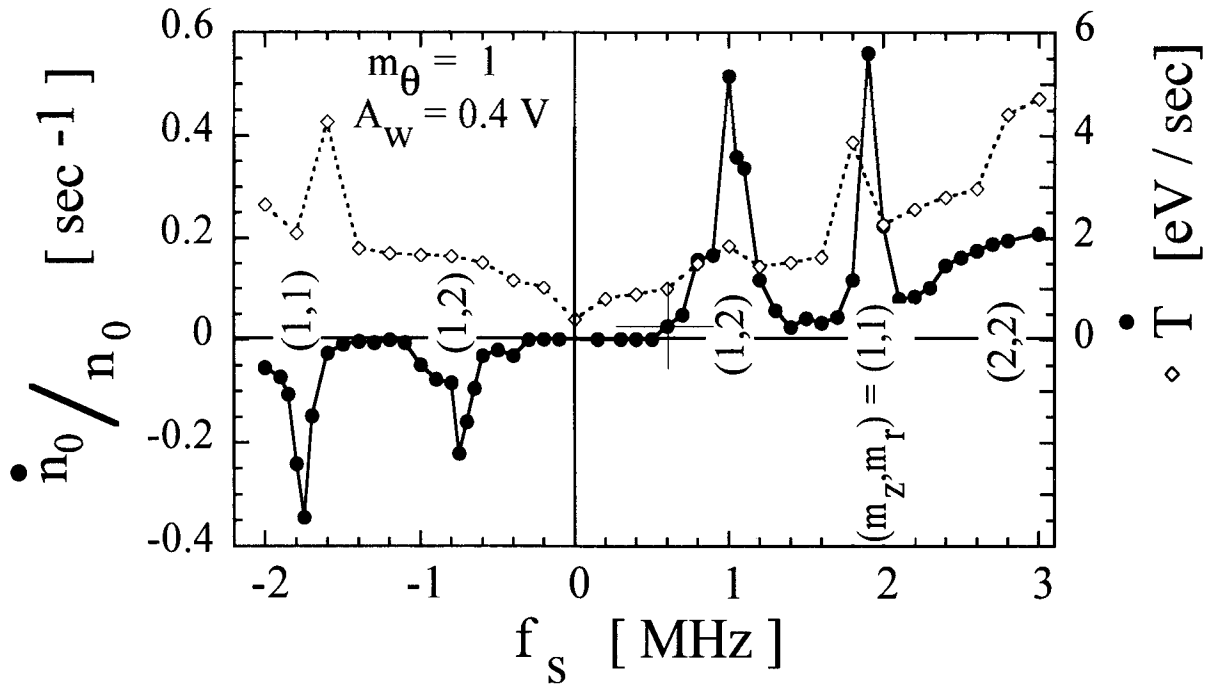

Fig. 2. Density compression rate for *strong* drive and plasma heating rate for $m_\theta = 1$ rotating drive. The compression peaks are associated with shifted (m_z, m_r) modes.

a *strong* drive of amplitude $A_w = 0.4$V is applied to the injected plasma profile. Here, an $m_\theta = 1$ rotating drive at a chosen frequency is applied to the sectored electrode S8 for 5 sec, and the initial compression (or expansion) rate $\dot{n}_0/n_0$ is measured. The measured background expansion rate of $(\dot{n}_0/n_0)_{\rm bkg} = -4\times10^{-3}$ sec^{-1} (somewhat less than expected from the n^2 scaling) has been subtracted from the data, so the plot indicates torque from the rotating drive alone. Two strong compression peaks and one broader compression region are observed; and two negative torque peaks are clearly visible in the reverse drive direction. Figure 2 also shows the rate of temperature change $\dot{T}$, suggesting that the drive causes general heating as well as heating directly associated with T-G mode resonances. These temperature changes shift and broaden the T-G modes, making precise comparison with theory difficult.

For comparison to linear mode theory, we apply a *weak* $m_\theta = 1$ rotating wall, with $A_w = 0.025$V. The resulting compression peaks are shown in Fig. 3. This small amplitude does not measurably heat the plasma, so the temperature remains low, with $T \approx 0.1 - 0.2$ eV. We observe many narrow T-G compression peaks, and these correspond closely with wave transmission peaks, i.e. 10–30dB enhancement in the wave signal received at S4. The observed wave transmission peaks correspond closely with numerical drift-kinetic predictions for T-G plasma modes varying as $h(r,m_r)\exp(im_\theta\theta + im_z\, z\pi/L_p)$ where $h(r,m_r)$ represents the radial eigenfunction with m_r zeros in the radial eigenfunction (counting the one at $r = 0$). The six observed wave transmission and plasma compression peaks agree quantitatively with the (m_z, m_r) mode frequencies calculated numerically using two "fit" parameters of $N_{\rm tot} = 2.7\times10^9$ and $T = 0.1$eV. These parameters are consistent with the measured $N_{\rm tot} = (3\pm0.6)\times10^9$ and $T = 0.1 - 0.2$eV. This correspondence has been further verified by varying the plasma length and by tailoring the antenna configuration to distinguish even and odd m_z.

The T-G modes for long columns within a cylindrical wall are predicted to have a rotationally-shifted "acoustic" dispersion relation, given approximately by

$$f - m_\theta f_R \approx \pm g(m_r,T)\,\frac{\omega_p}{2\pi}\,R_p\,\frac{\pi m_z}{L_p}\,. \qquad (1)$$

The left hand side of Eq. (1) represents the frequency of the mode in the plasma rotating frame f_R, which

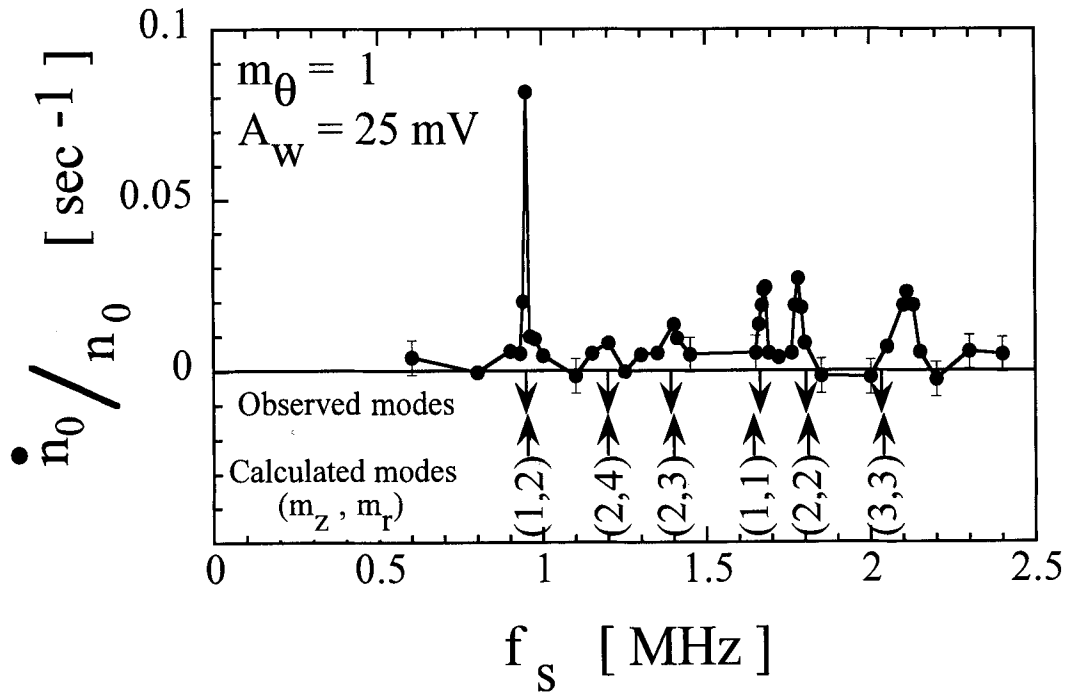

Fig. 3. Density compression rate for *weak* drive $m_\theta = 1$, compared to the observed and calculated Trivelpiece-Gould (T-G) plasma mode frequencies for various (m_z, m_r).

can be approximated by $f_R \approx f_E$ when the diamagnetic and centrifugal drift terms are small. The shifted frequencies are proportional to $N_{\rm tot}^{1/2}$ through $\omega_p \equiv [4\pi ne^2/m]^{1/2}$ and R_p, are proportional to $k_z \equiv \pi m_z/L_p$, and depend functionally on T and m_r. In contrast, the radial density profile $n(r)$ and absolute column size R_p have little effect on the mode frequencies except through f_R.

The observed compression peaks and wave transmission peaks are also consistent with Eq. (1) when the column length is varied. Changing L_p from 35 to 17.5 cm moved the first (1,2) compression peak of Fig. 2 from 1.0 to 1.8 MHz, and moved the (1,2) transmission peak from 0.97 to 1.75 MHz. Separate $m_\theta = 1$ wave transmission experiments agree reasonably well with Eq. (1) for $L_p = 17.5$ to 40.9 cm and $m_z = 1, 2$, $m_r = 1, 2$.

The rotating wall technique enables practical plasma manipulation; for example, Fig. 4 demonstrates plasma compression (solid dots) by slowly ramping the drive frequency from 0.5 to 2.13 MHz in 1000 seconds. From 0.5 MHz to 0.65 MHz, the central density slowly decreases, indicating that there is no significant torque from the rotating wall drive and that no torque-balanced equilibrium is reached. From 0.65 MHz to 1.95 MHz, the torque provided by the rotating wall coupling through the (1,2) mode exactly balances the background drags, and the plasma is in equilibrium. Above 1.95 MHz, the background drags are larger than the rotating wall torque, and the plasma expands rapidly before reaching a new equilibrium with torque coupled through the (2,2) mode.

The range of torque-balanced equilibria obtained in Fig. 4 is quantitatively explained by the compression peaks of Fig. 2 modified by the temperature- and density-induced shifts in mode frequencies. That is, the equilibria of Fig. 4 with $0.65 < f_s < 1.95$ and $4.5 < n_0 < 14$ represent a torque-balanced equilibrium "riding up" the left side of the (1,2) peak of Fig. 2; here, the increasing background drag $((\dot{n}_0/n_0)_{\rm bkg} \propto n_0^2)$ is balanced by the (increasing) drive torque as f_s approaches the resonant peak at $f^{m_\theta}_{m_z,m_r}$. The "crash" at $f_s = 2$ occurs because the drive at peak supplies insufficient torque, so the plasma expands until a new equilibrium is obtained on the left side of the next peak.

To see this quantitatively, we numerically calculate the shifted mode frequencies $f^{m_\theta}_{m_z,m_r}(n_0, T)$ appropriate to the measured n_0 and T during the compression ramp of Fig. 4. For example, a drive at $f_s = 0.95$ gives

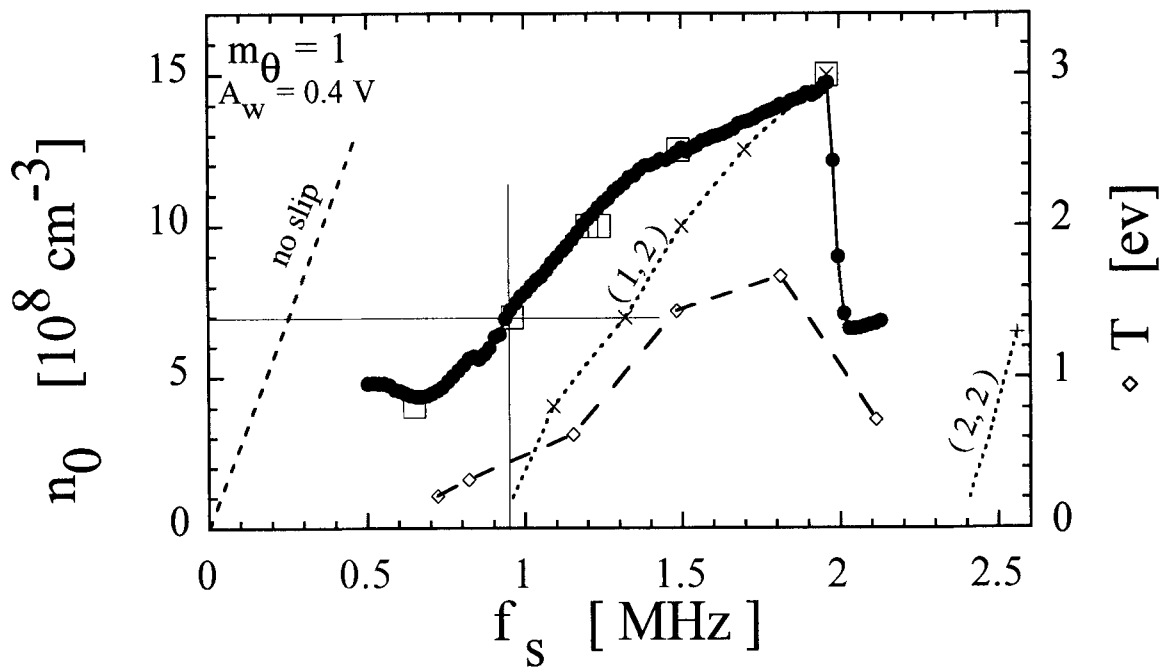

Fig. 4. Central density versus ramped rotating drive frequency f_s for $m_\theta = 1$ and measured temperature during the ramp.

a plasma density $n_0 = 7$ and temperature $T \approx 0.4$, and we calculate the resonant mode frequency to be $f^{(1)}_{(1,2)}(7, .4) = 1.32$ as shown by an X. The background drag on this plasma, $(\dot{n}_0/n_0)_{\rm bkg} \simeq 3 \times 10^{-2}{\rm sec}^{-1}$, approximately equals the torque represented by the first non-zero dot on Fig. 2, which is to the left of the (1,2) peak by an amount $\delta f \approx -0.4$. For simplicity, we presume that the (1,2) compression peak shifts in frequency so as to remain centered at $f^{(1)}_{(1,2)}(n_0, T)$; and that the peak maintains the same height and width. We then conclude that this (small) torque should be obtained at a drive frequency $f_s^{\rm tb} = f^{(1)}_{(1,2)} + \delta f = 0.95$, shown by the square in Fig. 4. The torque-balanced drive frequencies $f_s^{\rm tb}$ predicted by this construction closely agree with the actual ramp frequencies f_s over the range of equilibria shown. At the maximum density obtained($n_0 = 15$), δf is approximately zero, indicating that any further increase in f_s would move the equilibrium to the right-hand side of the (1,2) compression peak; but this side of the peak is unstable [12], leading to the crash. The plasma then expands and locks to a new equilibrium on the left side of the (2,2) mode.

The nonlinear nature of the coupling to the (1,1) mode is shown in Fig. 5. The measured compression rate (dots) scales as $\dot{n}/n_0 \propto A_w^{1.1}$ for the experimentally accessible range of $A_w \geq 0.025$V. To understand this result, we measured the amplitude $A_{\rm rec}$ of the received signal in a transmission experiment, and obtained scalings of $A_{\rm rec} \propto A_w^{1.1}$ for $A_w < 0.02$V and $A_{\rm rec} \propto A_w^0$ for $A_w > 0.03$V. Simple perturbation theory suggests that the compression should scale as $(\dot{n}/n_0) \propto \delta n \cdot \delta\psi \cdot \cos(\phi)$, where δn is the plasma density perturbation (with $\delta n \propto A_{\rm rec}$), $\delta\psi$ is the applied potential perturbation (with $\delta\psi \propto A_w$), and ϕ is the phase shift between δn and $\delta\phi$ (with measurements showing $\phi \approx$ const). Since the density perturbation δn is observed to be saturated for $A_w > 0.03$V, this theory perspective "predicts" that $\dot{n}_0/n_0 \propto A_w^1$, as observed experimentally.

We have interpreted the rotating wall coupling as a collective effect, in contrast with "side band cooling" which is interpreted as a single particle effect, i.e. the energy of a single particle transferred from the magnetron motion into damped axial or cyclotron motion.

Quadrupole rotating perturbations are also observed to couple to electron plasmas through $m_\theta = 2$, (m_r, m_z) Trivelpiece-Gould modes. Furthermore, recent experiments with pure ion plasma columns indicate that $k_z \neq 0$ Trivelpiece-Gould mode resonances are the dominant torque coupling mechanism.

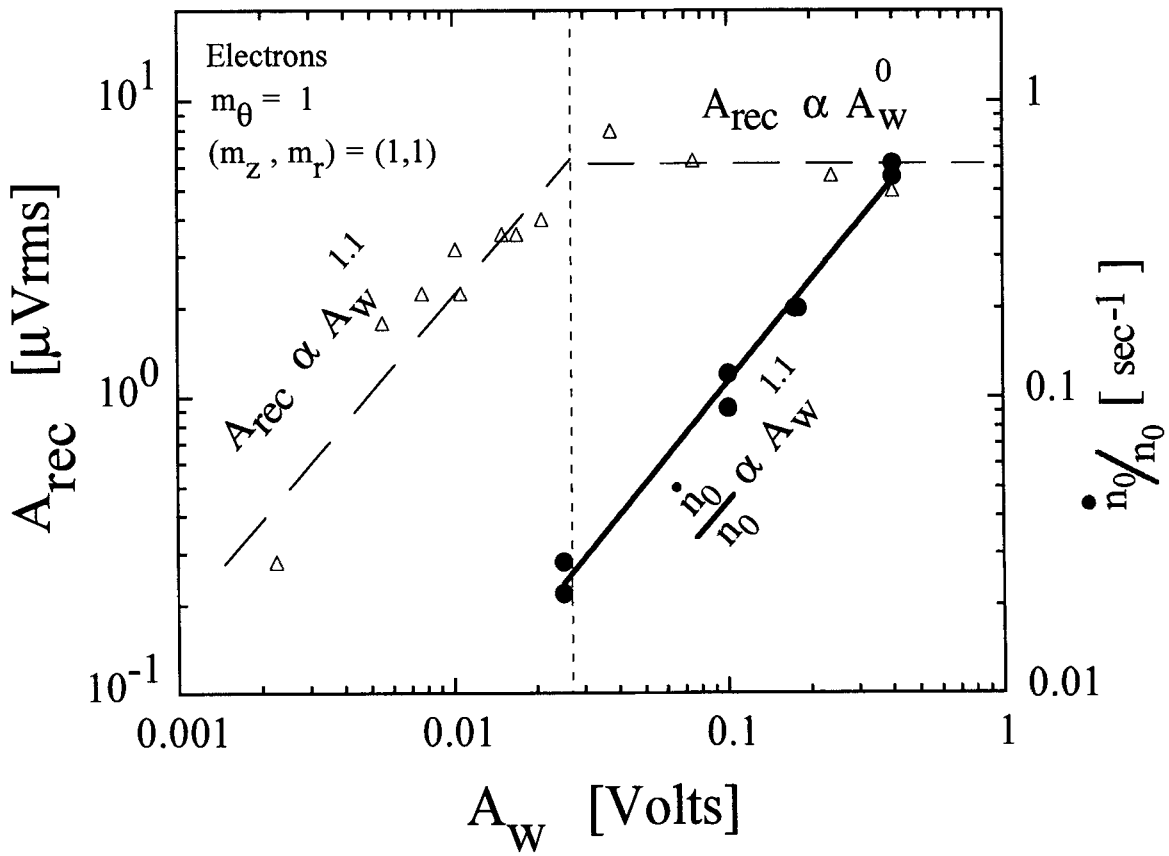

Fig. 5. Peak density compression rate and amplitude of the received signal on S4 for the $m_\theta = 1$, (1,1) mode driven by S8.

A rotating wall technique has also been applied to spheroidal ion crystals [13] using an axially uniform rotating electric field. Here, the torque is applied to a *solid* object, and in this "rotating brick" case, the crystal rotation was generally observed to be phase locked with the rotating field [13]. For an electron plasma, finite slip is required to apply a torque on the *fluid*; the T-G modes rotate faster (or slower) than the plasma, and the angular momentum carried by the wave is transferred to the particles. However, further experiments will be needed to clarify the distinction between the finite-slip $k_z \neq 0$ couplings described here and the zero slip $k_z = 0$ coupling obtained with spheroidal coulomb ion crystals [13]. Further, the wave-particle interaction which generates the torque is not understood theoretically: if the interaction is essentially Landau damping, the measurements imply that this damping is not in the linear regime. Further experiments may clarify this issue.

We thank Drs. Thomas M. O'Neil, Daniel H.E. Dubin, X.-P. Huang, Travis Mitchell, John J. Bollinger, Robert E. Pollock, and Mr. James Danielson for stimulating discussions, Dr. Ross Spencer for use of his drift kinetic computer code; and Mr. Robert Bongard for construction of a custom 8 channel digital function generator. This work is supported by Office of Naval Research Grant No. N00014-96-1-0239 and National Science Foundation Grant PHY94-21318.

REFERENCES

1. D.J. Heinzen, J.J. Bollinger, F.L. Moore, W.M. Itano, and D.J. Wineland, Phys. Rev. Lett. **66**, 2080 (1991).

2. D.S. Hall and G. Gabrielse, Phys. Rev. Lett. **77**, 1962 (1996); ATHENA Collaboration, Hyperfine Interactions **109**, 1 (1997).

3. D.L. Eggleston, T.M. O'Neil, and J.H. Malmberg, Phys. Rev. Lett. **53**, 982 (1984).

4. T.B. Mitchell, Ph.D. Thesis, UCSD (1993); see also T.B. Mitchell et al. in this book.

5. R.E. Pollock and F. Anderegg, in *Nonneutral Plasma Physics II*, AIP Conf. Proc. **31**, 139 (1995); R.E. Pollock, D. Stoller, A. Sarrazine, H. Gerberich, and T. Sloan, Bull. Am. Phys. Soc. **41**, 1603 (1996).

6. X.-P. Huang, F. Anderegg, E.M. Hollmann, C.F. Driscoll, and T.M. O'Neil, Phys. Rev. Lett. **78**, 875 (1997). Recent results on pure electron plasmas can be found in: F. Anderegg, E.M. Hollmann, and C.F. Driscoll,"Rotating Field Confinement of Pure electron Plasma Using Trivelpiece-Gould Mode," submitted to Phys. Rev. Lett.

7. F. Anderegg, X.-P. Huang, E. Sarid, and C.F. Driscoll, Rev. Sci. Instrum. **68**, 2367 (1997).

8. J.S. deGrassie and J.H. Malmberg, Phys. Fluids **23**, 63 (1980).

9. B.R. Beck, J. Fajans, and J.H. Malmberg, Phys. Plas. **3**, 1250 (1996); D.L. Eggleston, C.F. Driscoll, B.R. Beck, A.W. Hyatt, and J.H. Malmberg, Phys. Fluids B **4**, 2432 (1992).

10. C.F. Driscoll, K.S. Fine, and J.H. Malmberg, Phys. Fluids **29**, 2015 (1986).

11. S.A. Prasad and T.M. O'Neil, Phys. Fluids **26**, 665 (1983); A.W. Trivelpiece and R.W. Gould, J. Appl. Phys. **30**, 1784 (1959).

12. T.M. O'Neil and D.H.E. Dubin, Phys. Plasmas **5**, 2163 (1998).

13. X.-P. Huang, J.J. Bollinger, T.B. Mitchell, and W.M. Itano, Phys. Rev. Lett. **80**, 73 (1998).